ACS OMEGA

http://pubs.acs.org/journal/acsodf

Article

Growth of High-Purity and High-Quality Turbostratic Graphene with Different Interlayer Spacings

Phurida Kokmat, Piyaporn Surinlert, and Akkawat Ruammaitree*

Cite This: *ACS Omega* 2023, 8, 4010−4018

Read Online

ACCESS | Metrics & More | Article Recommendations | Supporting Information

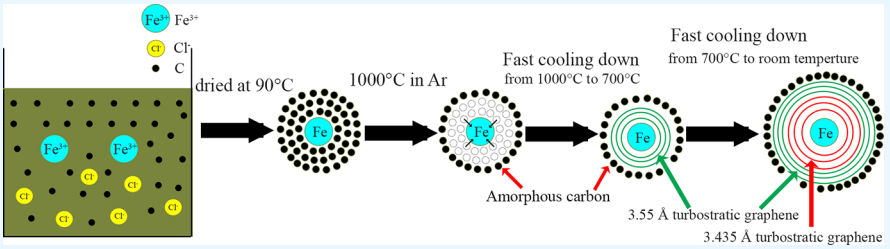

ABSTRACT: Turbostratic graphene is a multilayer graphene, which has exotic electrical properties similar to those of monolayer graphene due to the low interlayer interaction. Additionally, the stacking structure of the turbostratic multilayer graphene can decrease the effect of attachment of charge impurities and surface roughness. This paper explores the growth of high-purity and high-quality turbostratic graphene with different interlayer spacings by calcining ferric chloride and sucrose at 1000 °C for 1 h under an argon atmosphere. X-ray diffraction patterns and Raman results imply that the turbostratic graphene contains two different interlayer spacings: 3.435 and 3.55 Å. The 3.55 Å turbostratic graphene is on top of the 3.435 Å turbostratic graphene, and there is an AB stacking pattern between the topmost graphene layer of 3.435 Å turbostratic graphene and the first graphene layer of the 3.55 Å turbostratic graphene, with an interlayer spacing of 3.35 Å. The two different interlayer spacings of turbostratic graphene arise from different cooling rates between the higher temperature ranges (>700 °C) and lower temperatures (<700 °C).

1. INTRODUCTION

Monolayer graphene is a one-atom-thick layer, which consists of carbon atoms arranged in a hexagonal honeycomb lattice. The monolayer graphene has outstanding electrical properties such as a linear dispersion of carriers at the *K*-point[1,2] and high carrier mobility.[3−5] However, its exotic electrical properties are demoted due to the high level of attachment of charge impurities[6] and surface roughness.[7] The monolayer graphene may contain large amounts of charge impurities from surrounding environments and high surface roughness because its thickness is only one carbon atom thick, leading to the degradation of its electrical properties. Moreover, the large-scale synthesis of monolayer graphene is still challenging. Although multilayer graphene can decrease the effect of attachment of charge impurities and surface roughness due to the stacking structure and the large-scale production of multilayer graphene is facile, the electrical properties (such as carrier mobility) of multilayer graphene are lower than those of monolayer graphene due to the presence of interlayer coupling.

Turbostratic graphene consists of multilayer graphene, which has exotic electrical properties similar to those of monolayer graphene due to the relative rotations that decouple the electronic states of adjacent graphene layers.[8] In addition, the wideness of the interlayer spacing can also decrease the interlayer coupling. Hence, the turbostratic stacked multilayer graphene has great potential for high-performance electronic devices.

The methods for graphene synthesis have continually been improved to produce high-quality graphene with large-scale and low-cost production. In 2004, Novoselov et al. demonstrated the synthesis of graphene by micromechanical exfoliation of graphite.[9] This method achieved the high-quality single-layer graphene, but its production scale was very small. Epitaxial graphene growth on silicon carbide by thermal decomposition can produce large-scale and high-quality graphene,[10−12] whereas this procedure is only suitable for the synthesis of a graphene film on semiconductors because the graphene film can directly be grown on silicon carbide. Chemical vapor deposition (CVD) is a popular method of synthesizing large-scale and large-area graphene films with low-cost production.[13−15] For the synthesis of graphene powder, the oxidation−reduction method is widely utilized to fabricate reduced graphene oxide with large-scale and low-cost

Received: October 23, 2022
Accepted: January 13, 2023
Published: January 22, 2023

https://doi.org/10.1021/acsomega.2c06834
ACS Omega 2023, 8, 4010−4018

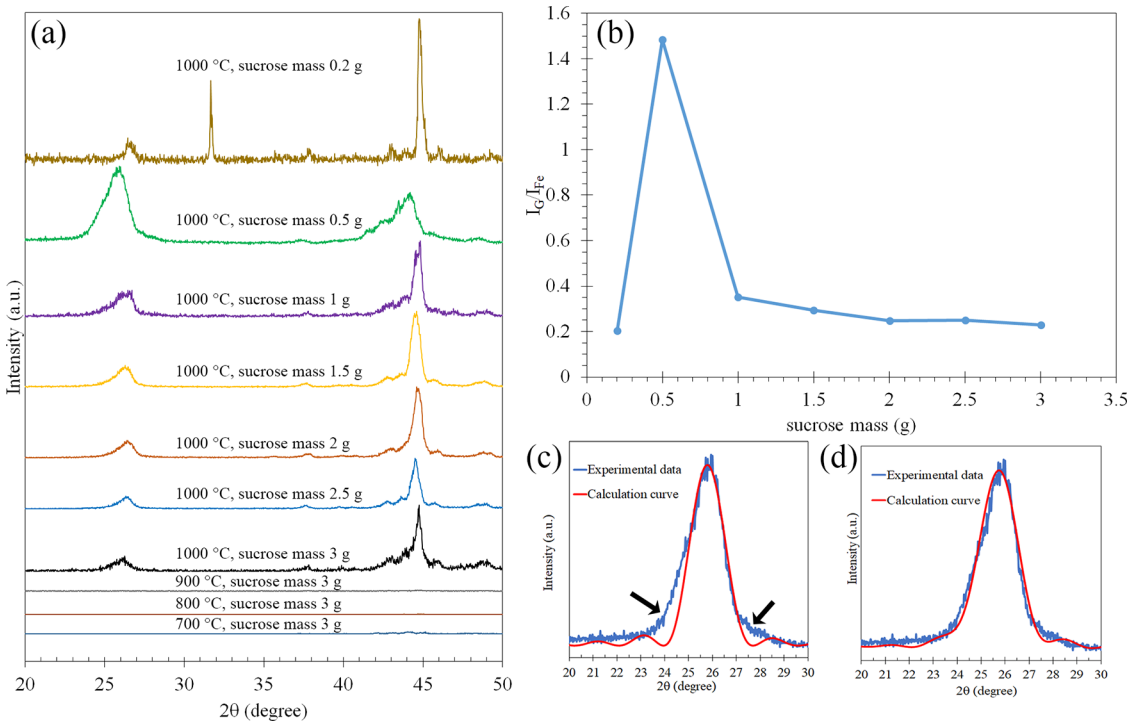

Figure 1. (a) XRD patterns of the samples calcined at 700−1000 °C using 0.2−3 g of sucrose. (b) Relationship between the intensity ratio of the graphene peak to the iron peak (I_G/I_{Fe}) and sucrose mass of samples calcined at 1000 °C. (c,d) XRD experimental results (blue) and XRD fitting curve (red) of the 0.5 g sample at the graphene peak. The fitting curve was calculated using the original equation (c) and the modified equation (d). Black arrows indicate large misfit positions.

production.[16−18] However, the electrical properties of the reduced graphene oxide are poor due to the appearance of a large number of defects and the oxygen content on its surface. For the synthesis of a turbostratic graphene film, Wei et al. modified the CVD method for the growth of a turbostratic graphene film by growing another graphene on top of single-layer graphene.[19] Garlow et al. grew the large-area turbostratic graphene on Ni(111) using physical vapor deposition.[8] Liu et al. synthesized turbostratic graphene via negative carbon ion implantation.[20] In the case of turbostratic graphene powder, Athanasiou et al. showed the growth of turbostratic graphene powder using a laser-assisted process.[21] The flash Joule heating process is a new method for synthesizing turbostratic graphene powder by compressing the carbon source to increase its temperature to higher than 3000 K in less than 100 ms.[22,24] However, the flash Joule heating system has a risk of electrical shock or electrocution. Hu et al. demonstrated the growth of turbostratic graphene powder using concentrated solar radiation.[25] Even if this method is simple, rapid, and environment-friendly, the quality of resultant turbostratic graphene is low. In our previous report, we demonstrated the growth of high-quality turbostratic graphene powder by calcining the mixture of ferric chloride and sucrose at 700 °C under argon flow for 6 h.[26] The resultant turbostratic graphene contained a constant interlayer spacing of 3.43 Å.

The current study investigates the growth of high-purity and high-quality turbostratic graphene with different interlayer spacings by calcining ferric chloride and sucrose at high temperatures for 1 h under an argon atmosphere. This is a simple and cost-effective method for the mass production of high-purity turbostratic graphene with different layer spacings. In addition, we modified the model for X-ray diffraction (XRD) curve fitting. The modified model can reveal the proportion of graphene with different interlayer spacings. The structure and proportion of turbostratic graphene and AB-stacked graphene are investigated by XRD and Raman spectroscopy. X-ray photoelectron spectroscopy (XPS) is utilized to study the growth mechanism of the turbostratic graphene.

2. EXPERIMENTAL SECTION

2.1. Preparation of Turbostratic Graphene. $FeCl_3$ (3 g) and sucrose (0.2−3 g) were dissolved in 5 mL of deionized water. The solution was stirred for 20 min before being poured into a porcelain combustion boat. After that, the solution was dried in an oven for 24 h at 90 °C. Thereafter, the samples were calcined at 700−1000 °C for 1 h in a quartz tube furnace under an argon atmosphere with the argon flow rate of 700 sccm (a photograph of the graphene calcination station is shown in Figure S1 in the Supporting Information). The average heating rate of the furnace from room temperature to 1000 °C was 13.5 °C/min. After that, the sample was cooled down under argon flow by opening the furnace as shown in Figure S1. When the furnace was opened, the quartz tube's top half contacted with air, while its bottom half contacted with the hot furnace, resulting in cooling rates at higher temperatures being faster than at low temperatures. After cooling down, the samples, composed of graphene-wrapped iron, were retrieved. The iron inside was removed by soaking the sample in 6 M HCl. The names of samples were designated by the sucrose quantity; for example, "0.5 g sample" means that this sample was grown by calcining the mixture of 0.5 g of sucrose, 3 g of $FeCl_3$, and 5 mL of deionized water at 1000 °C for 1 h under an argon atmosphere.

2.2. Characterization. XRD patterns were recorded by a benchtop X-ray powder diffractometer (Bruker) using Cu Kα

https://doi.org/10.1021/acsomega.2c06834
ACS Omega 2023, 8, 4010−4018

Table 1. Parameters for XRD Curve Fitting

calculation method	peak number	A	d (Å)	β_0	β_1	β_2	β_3	β_4	β_5	β_6	β_7	β_8	β_9	β_{10}	β_{11}	β_{12}	β_{13}
original equation	1		3.45	1	1	1	1	1	1	1	1	1	1	1	1	1	1
modified equation	1	0.5	3.35	1	1	1	1	1	1	1	0.5	0.5					
	2	1	3.435	1	1	1	1	1	1	1	1	1	1	1	1	1	1
	3	1	3.55	1	1	1	1	1	1	1	1	0.5	0.5	0.5	0.5	0.5	

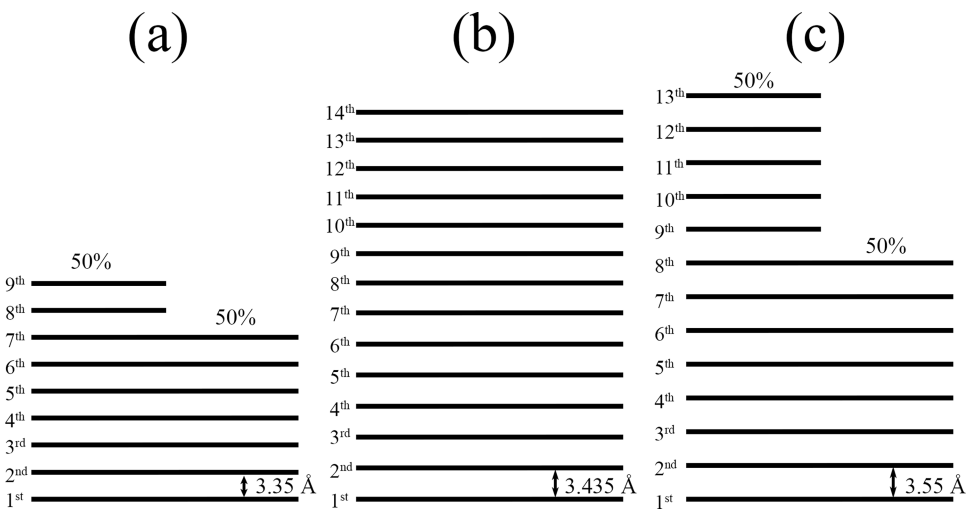

Figure 2. Graphene structure in the 0.5 g sample. (a) Structure of AB-stacked graphene. (b,c) Structure of turbostratic graphene with interlayer spacings of 3.435 and 3.55 Å, respectively.

radiation (λ = 0.154184 nm). Field-emission scanning electron microscope images were acquired by analysis of the samples using a Hitachi SU8010, operating at an accelerating voltage of 20 kV. Raman measurement was performed on a Horiba instrument in the range of 1300−2800 cm^{-1} at room temperature. The wavelength and spot size of laser excitation were 532 nm and ∼1 μm, respectively. XPS was performed under the base pressure of ∼2 × 10^{-9} Torr using an Axis Supra, Kratos with a 225 W Al Kα monochromator.

3. RESULTS AND DISCUSSION

After the calcination process, the structures of the samples, composed of graphene-wrapped iron, were investigated by XRD. Figure 1a shows XRD results of the samples after calcination at 700−1000 °C for 1 h. For the samples calcined at 1000 °C, the XRD patterns display two significant peaks at ∼26 and ∼44°, corresponding to the diffraction from the (002) plane of graphene and the (110) plane of iron,[27] respectively. In addition, the peak intensity ratio of graphene to iron (I_G/I_{Fe}) of the samples calcined at 1000 °C increases with the reduction of the sucrose mass (Figure 1b), implying that the purity of graphene increases when the mass ratio of sucrose to ferric chloride decreases. The XRD pattern of the 0.5 g sample displays the highest I_G/I_{Fe}, indicating that this sample contains the highest purity of graphene. However, the XRD pattern of the 0.2 g sample shows the lowest I_G/I_{Fe}, revealing that the graphene quantity is limited by the sucrose mass. Figure 1c shows curve fitting on the experimental XRD patterns at the graphene peak of the 0.5 g sample. The fitting curve is calculated using the following original equation from ref 28:

$$I \propto |f(\theta)|^2 \left| \sum_{j=0}^{N-1} \beta_j e^{ika_j} \right|^2 \quad (1)$$

where I is the XRD intensity. $f(\theta)$ is the atomic scattering of carbon.[29] N is the layer number of graphene. β_j is the occupancy of the $(j + 1)$th graphene layer. $ka_j = (4\pi d_j \sin(\theta))/\lambda$ where d_j is the interlayer spacing of graphene. θ is the incident angle. λ is the wavelength of the incident X-ray beam. The best fitting curve is calculated using parameters in Table 1. However, the fitting curve displays the large misfit between experimental data and the calculation curve, implying that the 0.5 g sample contains graphene with various interlayer spacings. Therefore, the original equation (eq 1) should be modified to the following equation:

$$I \propto |f(\theta)|^2 \left| A_1 \sum_{j=0}^{N_1-1} \beta_j e^{ika_j} + A_2 \sum_{j=0}^{N_2-1} \beta_j e^{ika_j} + A_3 \sum_{j=0}^{N_3-1} \beta_j e^{ika_j} \right|^2 \quad (2)$$

where A_1, A_2, and A_3 are the proportion of graphene with different interlayer spacings. The modified fitting curve (Figure 1d) is calculated using the parameters shown in Table 1. The well fitting curve reveals that the proportions of graphene with interlayer spacings of 3.35, 3.435, and 3.55 Å in the 0.5 g sample are 20, 40, and 40%, respectively. Generally, the stacking type and the interlayer spacing of graphene are AB stacking and 3.35 Å, respectively. The interlayer spacings of 3.435 and 3.55 Å are much wider than those of AB-stacked graphene, implying that the stacking type of graphene is turbostratic stacking.[30] Additionally, the fitting curve reveals information on thickness distribution of graphene shown in

https://doi.org/10.1021/acsomega.2c06834
ACS Omega 2023, 8, 4010−4018

Figure 2. Therefore, the graphene thickness and its proportion in the 0.5 g sample can be estimated and are shown in Table 2.

Table 2. Information on the Graphene Structure and Proportion in the 0.5 g Sample

graphene thickness	interlayer spacing	stacking type	proportion
7 layers	3.35 Å	AB stacking	10%
8 layers	3.55 Å	turbostratic stacking	20%
9 layers	3.35 Å	AB stacking	10%
13 layers	3.55 Å	turbostratic stacking	20%
14 layers	3.435 Å	turbostratic stacking	40%

Figure 3 displays SEM images of the samples calcined at 1000 °C. The SEM images show that the graphene-wrapped iron powder gathers and forms a big cluster in the case of the sample prepared using a high quantity of sucrose. The size of sample particles decreases when the sucrose mass reduces.

The Raman spectrum of the 0.5 g sample (Figure 4a) displays the characteristic peaks of graphene at 1572 (G band) and 2684 cm^{-1} (2D band). The G band and the 2D band arise from the E_{2g} vibrational mode and the second-order two-phonon mode, respectively.[31] Therefore, the appearance of the G band and the 2D band confirms the presence of graphene in the 0.5 g sample. The intensity ratio of the G peak to the 2D peak (I_G/I_{2D}) is more than 1. This corresponds with the turbostratic graphene prepared by direct carbon ion implantation[20] and a laser-assisted process.[21] On the other hand, this I_G/I_{2D} differs from the turbostratic graphene synthesized via physical vapor deposition[8] displaying that the I_G/I_{2D} was less than 1. However, Casiraghi found that the intensity of the G peak is independent of doping, while the intensity of the 2D peak considerably depends on the doping, i.e., the intensity of the 2D peak rapidly decreases with the increment of doping.[32] Therefore, the turbostratic graphene prepared by different methods may contain different doping amounts. In addition, the Raman spectrum shows the D band at 1341 cm^{-1}. The D band arises from the sp^2-hybridized disordered carbon materials.[33] The intensity ratio of the D peak to the G peak (I_D/I_G) is widely utilized to identify the crystalline quality of graphene.[34] Figure S2a shows the Raman spectra of the samples annealed at 1000 °C. The I_D/I_G values of these samples tend to decrease with the reduction of the sucrose mass (Figure S2b). However, the I_D/I_G of the 0.2 g sample is higher than those of the 0.5 g sample, 1 g sample, 1.5 g sample, and 2 g sample due to a lack of carbon in the carbon oxidation process[35,36] at high temperatures resulting in a large amount of oxygen remaining in the sample. The presence of oxygen impedes the growth of graphene,[37] leading to the low crystalline quality of graphene. The 0.5 g sample has the lowest I_D/I_G, which is in the range from 0.061 to 0.110 (Figure S2c). The average I_D/I_G of the 0.5 g sample is 0.086, which is smaller than the value (I_D/I_G = 0.23) observed from the turbostratic graphene prepared by calcining at 700 °C for 6 h,[26] implying that calcination using higher temperatures can improve the crystallinity of graphene. In addition, this value is much smaller than the I_D/I_G of turbostratic graphene prepared by CVD,[19] direct carbon ion implantation,[20] laser-assisted method,[21] flash Joule heating,[22−24] and concentrated solar radiation,[25] which showed the following I_D/I_G: 0.36, 1.2−1.7, 0.9−1.1, 0.12−0.81,

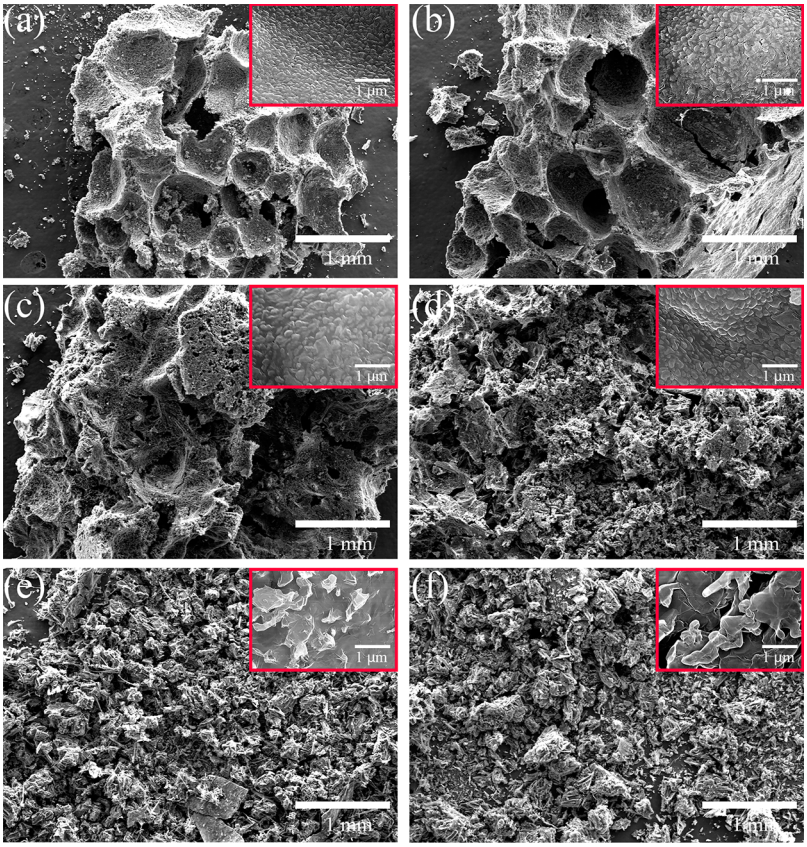

Figure 3. SEM images of the 3 g sample (a), 2.5 g sample (b), 2 g sample (c), 1.5 g sample (d), 1 g sample (e), and 0.5 g sample (f). The inset displays a magnified image measured at the center of each image.

https://doi.org/10.1021/acsomega.2c06834
ACS Omega 2023, 8, 4010−4018

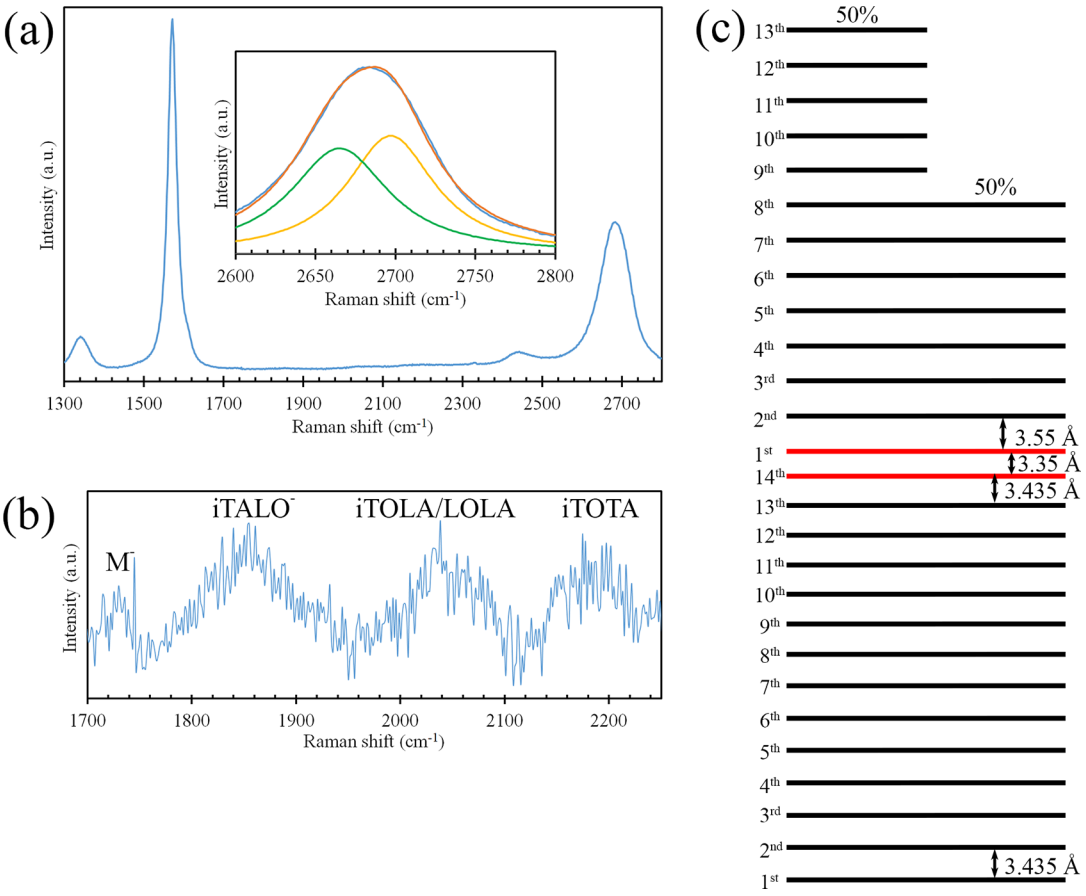

Figure 4. (a) Raman spectrum of the 0.5 g sample. The inset shows the curve fitting (orange) on the experimental Raman spectrum (blue) at the 2D band. The fitting curve is calculated by summation of 2 Lorentzian functions, which originate from turbostratic graphene with interlayer spacings of 3.435 and 3.55 Å. (b) Magnified Raman spectrum of the 0.5 g sample between 1700 and 2300 cm^{-1}. (c) Structure of turbostratic graphene in the 0.5 g sample.

and ~0.8, respectively, indicating that the 0.5 g sample contains the highest crystalline quality of graphene. Moreover, the I_D/I_G is widely used to calculate the grain size of graphene (L_a) using the following equation:[38]

$$L_a\ (\mathrm{nm}) = (2.4 \times 10^{-10})\lambda_{laser}^4 \left(\frac{I_D}{I_G}\right)^{-1} \quad (3)$$

where λ_{laser} is the wavelength of the incident laser. The graphene grain size of the 0.5 g sample was shown to be about 223.5 nm. Figure 4a (inset) shows the curve fitting at the 2D band. In general, the 2D band of turbostratic graphene can be fitted by a single Lorentzian function, the same as monolayer graphene.[39] In the case of the 0.5 g sample, the 2D band was fitted by 2 Lorentzian functions at 2665 cm^{-1} with the full width at half-maximum (FWHM) of 75 cm^{-1} (green curve) and at 2697 cm^{-1} with the FWHM of 67 cm^{-1} (yellow curve). The peak area ratio of the yellow curve to the green curve was 1, which corresponded to XRD results and revealed the proportion of the graphene interlayer spacing for 3.55 to 3.435 Å (A_3/A_2) to be 1.

The iTALO$^-$ mode arises from a combination of in-plane transverse acoustic (iTA) and longitudinal optic (LO) phonons.[40,41] In some publications, the iTALO$^-$ mode and iTOLA/LOLA modes are designated as TS_1 and TS_2, respectively.[8,22,24] The 0.5 g sample contains the iTALO$^-$ peak at ~1850 cm^{-1} (Figure 4b). Generally, the intensity of the iTALO$^-$ peak is high in the case of monolayer graphene and turbostratic graphene, but it drastically decreases when the number of layers of graphene increased. For AB-stacked few-layer graphene, the peak intensity of iTALO$^-$ is extremely low, and it vanishes in the case of bulk highly ordered pyrolytic graphite (HOPG).[41] Thus, the presence of iTALO$^-$ reveals that the 0.5 g sample contains the turbostratic graphene. It corresponds with the XRD results.

The M band is an overtone of the oTO phonon, which was a result of the strong coupling between graphene layers that resulted in the M band appearing at ~1750 cm^{-1} for AB-stacked few-layer graphene and HOPG[41] but vanishing in the case of monolayer graphene and turbostratic graphene.[22,24] However, Gupta et al. proved that the M band can appear with the iTALO$^-$ band in the case of medium turbostratic graphene.[42] For the 0.5 g sample, the Raman spectrum displayed an absence of the M band, indicating that the structure of graphene was highly turbostratic stacking. However, the Raman spectrum showed the M$^-$ band at ~1730 cm^{-1}. In general, the M$^-$ band appears with the iTALO$^-$ in the case of AB-stacked bilayer graphene. The intensity of the M$^-$ band is higher than that of the iTALO$^-$ band.[41] For the 0.5 g sample, the Raman spectrum showed that the intensity of the M$^-$ band is lower than that of the iTALO$^-$ band, indicating that AB-stacked bilayer graphene and turbostratic graphene were in the same area. Therefore, the structure of turbostratic graphene in the 0.5 g sample can be

https://doi.org/10.1021/acsomega.2c06834
ACS Omega 2023, 8, 4010−4018

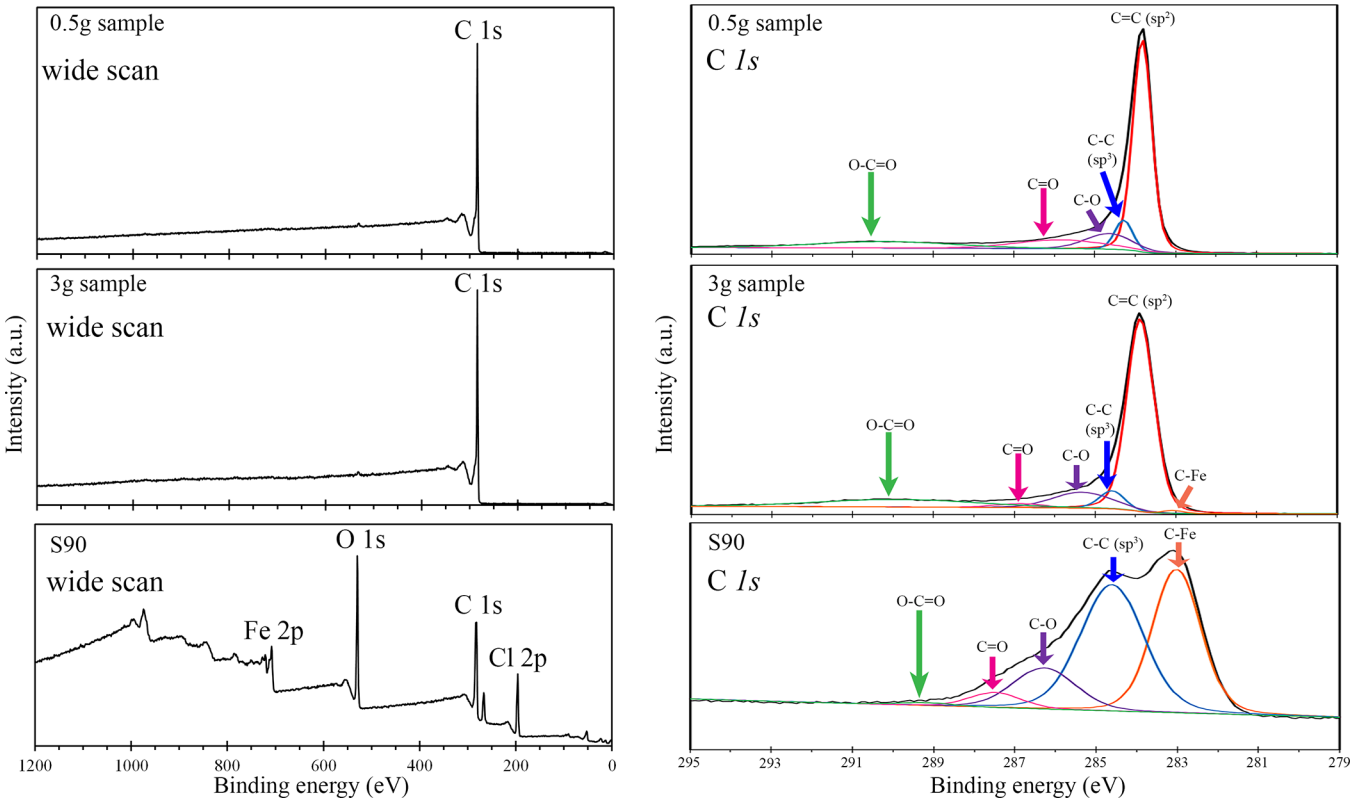

Figure 5. Wide-scan (left) and C 1s (right) XPS spectra of the 3 g sample before (S90) and after the calcination process and the 0.5 g sample after the calcination process.

described that the 3.55 Å turbostratic graphene is on top of the 3.435 Å turbostratic graphene. The stacking pattern between the topmost graphene layer of 3.435 Å turbostratic graphene and the first graphene layer of the 3.55 Å turbostratic graphene is AB stacking with the interlayer spacing of 3.35 Å (Figure 4c). The presence of two different types of interlayer spacings of turbostratic graphene is attributed to the large difference in cooling rates. The sample cooled quickly since when the furnace was opened, the top half of the quartz tube was in contact with air, while its bottom half was still in contact with the hot furnace, resulting in the cooling rate at high temperatures (>700 °C) being faster than that at low temperatures (<700 °C). The structure of turbostratic graphene in the 0.5 g sample differs from that of turbostratic graphene prepared by calcining at 700 °C for 6 h, as shown in our previous report.[26] The turbostratic graphene prepared by calcining at 700 °C contained a constant interlayer spacing of 3.43 Å. However, this value is close to the interlayer spacing of the 3.435 Å turbostratic graphene in the 0.5 g sample, implying that the faster cooling rate from 1000 to 700 °C caused a widening of the interlayer spacing. In addition, the structure of turbostratic graphene in the 0.5 g sample also differs from that of turbostratic graphene prepared by flash Joule heating[22] and concentrated solar radiation,[25] which reported that the resultant turbostratic graphene contains constant interlayer spacings of 3.45 and ∼3.81 Å, respectively.

Figure 5 shows wide-scan and C 1s XPS spectra of the 3 g sample before (S90) and after the calcination process and the 0.5 g sample after the calcination process. For S90, after dehydration at 90 °C for 24 h, the wide-scan XPS spectrum shows peaks of Cl, C, O, and Fe at ∼200, ∼285, ∼530, and ∼720 eV, respectively. For the C 1s XPS spectrum, the deconvolution displays peaks of C−Fe, C−C (sp^3), C−O, C═O, and O−C═O bonds at 283.0, 284.6, 286.3, 287.5, and 289.1 eV, respectively. The XPS spectrum shows a high peak area of C−Fe. The peak area ratio of the C−Fe bond to the C−C bond is 0.87. The XPS results imply that dehydration makes the amorphous carbon surround the iron, and the C−Fe bonding occurs between the iron and its nearest neighbor carbon atoms. After calcination at 1000 °C under argon flow for 1 h, the wide-scan XPS spectrum shows a tiny peak of O 1s and a high-intensity peak of C 1s. The C 1s XPS spectrum of the 3 g sample shows a prominent peak of the C═C (sp^2) bond at 283.9 eV. C═C (sp^2) corresponds to the π-bonded carbon atoms of the graphene network.[43] The peak areas of C−O and C═O bonds were significantly reduced, owing to carbon oxidation. The tiny peak area of C−Fe is still present. In the case of the 0.5 g sample, the C−Fe bond disappears from the XPS spectrum, implying that there is no C−Fe bonding between iron and the first carbon layer. Thus, the first carbon layer is the graphene layer.

Sample dehydration before calcination is an important process for growing the high-purity turbostratic graphene. The slow dehydration increases the amount of amorphous carbon atoms, which surround the iron atoms before the calcination. These surrounding amorphous carbon atoms are dissolved into the iron when the sample is annealed at 1000 °C under an argon atmosphere and form graphene after cooling down to room temperature. Figure S3a shows XRD patterns of the 0.5 g sample prepared with and without dehydration. The I_G/I_{Fe} values of the 0.5 g sample prepared with and without dehydration are 1.41 and 0.34, respectively, implying that the purity of turbostratic graphene prepared with dehydration is higher than that of turbostratic graphene prepared without

https://doi.org/10.1021/acsomega.2c06834
ACS Omega 2023, 8, 4010−4018

dehydration. The iron inside the sample can be removed by soaking the sample in 6 M HCl. The XRD pattern of the 0.5 g sample after immersion in HCl is also displayed in Figure S3a. The diffraction from the (110) plane of iron (~44°) disappears, indicating the absence of iron inside the sample. Yield is an important metric for the synthesis of graphene powder in mass production. In this report, the yield of graphene production was calculated using the ratio of mass of graphene powder to the mass of carbon in sucrose. Therefore, the yield of the 0.5 g sample was 56.19%. The reduction of yield arises from the loss of carbon atoms in the carbon oxidation process at high temperatures.

In addition, the cooling process is also important for the growth of turbostratic graphene. The effect of cooling on the growth of turbostratic graphene was studied by comparing the 0.5 g sample prepared at slow and fast cooling rates. In the case of the slow cooling rate, the 0.5 g sample was cooled down without opening the lid of the furnace. Figure S3b displays that the 0.5 g sample's XRD diffraction peaks of graphene prepared at fast and slow cooling rates shifted from ~26 to ~26.5, indicating that the average interlayer spacings of graphene decreased from 3.43 to 3.36 Å, respectively. This confirms that the growth of turbostratic graphene depends on the cooling rate.

Figure 6 provides a schematic presentation of the growth mechanism of turbostratic graphene with different interlayer

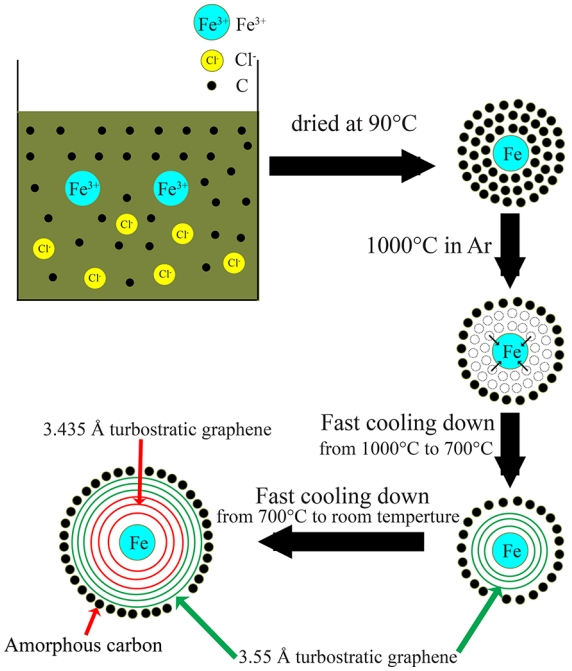

Figure 6. Growth mechanism of turbostratic graphene with 2 different interlayer spacings of 3.435 and 3.55 Å.

spacings. First, ferric chloride and sucrose are dissolved in deionized water. After dehydration at 90 °C for 24 h, the iron is enclosed by amorphous carbon atoms. C−Fe bonding occurs between the iron and its nearest neighbor carbon atoms. When the sample is annealed at 1000 °C for 1 h under argon flow, the surrounding carbon atoms are dissolved into the iron. Subsequently, the sample is fast cooled down to room temperature. When the sample is cooled down from 1000 to 700 °C, some dissolved carbon atoms in the iron precipitate and form turbostratic graphene with the interlayer spacings of 3.55 Å enclosing the iron. After the sample was cooled down from 700 °C to room temperature, the residual dissolved carbon atoms in the iron precipitate and form turbostratic graphene with the interlayer spacings of 3.435 Å enclosing the iron. The formation of turbostratic graphene with two different interlayer spacings is associated with different cooling rates. Athanasiou et al. stated that the formation of turbostratic graphene arises from the fast heating and cooling rates.[21] However, our results prove that the formation of turbostratic graphene arises from the fast cooling rate only. In addition, the remaining carbon atoms become amorphous and surround the turbostratic graphene. Hence, the preparation of samples using excess sucrose reduces the purity of graphene in the sample due to the formation of amorphous carbon.

4. CONCLUSIONS

We have studied the growth of turbostratic graphene with different interlayer spacings by calcining the mixture of sucrose and ferric chloride at 1000 °C for 1 h under an argon atmosphere. XRD results show that the purity of graphene depends on the quantity of sucrose. In addtion, the XRD pattern of the 0.5 g sample reveals the presence of graphene with interlayer spacings of 3.35, 3.435, and 3.55 Å. Moreover, the 2D band of the Raman spectrum can be fitted by two Lorentzian functions confirming that the 0.5 g sample contains turbostratic graphene with two different interlayer spacings of 3.435 and 3.55 Å. In addition, the Raman spectrum shows that the intensity peak of the M^- band is lower than that of the $iTALO^-$ band, implying that the 3.55 Å turbostratic graphene is on top of the 3.435 Å turbostratic graphene. In addition, the stacking pattern between the topmost graphene layer of 3.435 Å turbostratic graphene and the first graphene layer of the 3.55 Å turbostratic graphene is AB stacking with the interlayer spacing of 3.35 Å. The two different interlayer spacings of turbostratic graphene arise from different cooling rates between the range of higher temperatures (>700 °C) and lower temperatures (<700 °C).

■ ASSOCIATED CONTENT

Supporting Information

The Supporting Information is available free of charge at https://pubs.acs.org/doi/10.1021/acsomega.2c06834.

Photograph of graphene calcination station; Raman results of the samples calcined at 1000 °C using 0.2−3 g of sucrose; XRD patterns of the 0.5 g sample prepared without and with a dehydration process and the XRD pattern of the 0.5 g sample after immersion in HCl; XRD patterns of the 0.5 g sample prepared with a fast cooling rate and a slow cooling rate (PDF)

■ AUTHOR INFORMATION

Corresponding Author

Akkawat Ruammaitree − *Department of Physics, Faculty of Science and Technology, Thammasat University, Pathum Thani 12120, Thailand; Thammasat University Research Unit in Synthesis and Applications of Graphene, Thammasat University, Pathum Thani 12120, Thailand;* orcid.org/0000-0003-3753-6653; Email: u4605070@hotmail.com

https://doi.org/10.1021/acsomega.2c06834
ACS Omega 2023, 8, 4010−4018

Authors

Phurida Kokmat − *Department of Physics, Faculty of Science and Technology, Thammasat University, Pathum Thani 12120, Thailand*

Piyaporn Surinlert − *Chulabhorn International College of Medicine, Thammasat University, Pathum Thani 12120, Thailand; Thammasat University Research Unit in Synthesis and Applications of Graphene, Thammasat University, Pathum Thani 12120, Thailand*

Complete contact information is available at: https://pubs.acs.org/10.1021/acsomega.2c06834

Notes

The authors declare no competing financial interest.

■ ACKNOWLEDGMENTS

This work was supported by the Thailand Science Research and Innovation Fundamental Fund, Thammasat Univeristy Research Fund, contract no. TUFT-FF 51/2565, and Thammasat University Research Unit in Synthesis and Applications of Graphene.

■ REFERENCES

(1) Ohta, T.; Bostwick, A.; McChesney, J. L.; Seyller, T.; Horn, K.; Rotenberg, E. Interlayer Interaction and Electronic Screening in Multilayer Graphene Investigated with Angle-Resolved Photoemission Spectroscopy. *Phys. Rev. Lett.* **2007**, *98*, No. 206802.

(2) Emtsev, K. V.; Speck, F.; Seyller, T.; Ley, L.; Riley, J. D. Interaction, growth, and ordering of epitaxial graphene on SiC{0001} surfaces: A comparative photoelectron spectroscopy study. *Phys. Rev. B* **2008**, *77*, No. 155303.

(3) Geim, A. K.; Novoselov, K. S. The rise of graphene. *Nat. Mater.* **2007**, *6*, 183−191.

(4) Bolotin, K. I.; Sikes, K. J.; Jiang, Z.; Klima, M.; Fudenberg, G.; Hone, J.; Kim, P.; Stormer, H. L. Ultrahigh electron mobility in suspended graphene. *Solid State Commun.* **2008**, *146*, 351.

(5) Morozov, S. V.; Novoselov, K. S.; Katsnelson, M. I.; Schedin, F.; Elias, D. C.; Jaszczak, J. A.; Geim, A. K. Giant Intrinsic Carrier Mobilities in Graphene and Its Bilayer. *Phys. Rev. Lett.* **2008**, *100*, No. 016602.

(6) Yang, J.; He, Y.; Zhang, X.; Yang, W.; Li, Y.; Li, X.; Chen, Q.; Chen, X.; Du, K.; Yan, Y. Improving the electrical conductivity of copper/graphene composites by reducing the interfacial impurities using spark plasma sintering diffusion bonding. *J. Mater. Res. Technol.* **2021**, *15*, 3005−3015.

(7) Touski, S. B.; Hosseini, M. A Comparative Study of Substrates Disorder on Mobility in the Graphene Nanoribbon: Charged Impurity, Surface Optical Phonon, Surface Roughness. *Phys. E* **2020**, *116*, No. 113763.

(8) Garlow, J. A.; Barrett, L. K.; Wu, L.; Kisslinger, K.; Zhu, Y.; Pulecio, J. F. Large-Area Growth of Turbostratic Graphene on Ni (111) via Physical Vapor Deposition. *Sci. Rep.* **2016**, *6*, 19804.

(9) Novoselov, K. S.; Geim, A. K.; Morozov, S. V.; Jiang, D.; Zhang, Y.; Dubonos, S. V.; Grigorieva, I. V.; Firsov, A. A. Electric Field Effect in Atomically Thin Carbon Films. *Science* **2004**, *306*, 666−669.

(10) Hu, H.; Ruammaitree, A.; Nakahara, H.; Asaka, K.; Saito, Y. Few-layer epitaxial graphene with large domains on C-terminated 6H-SiC. *Surf. Interface Anal.* **2012**, *44*, 793−796.

(11) Ruammaitree, A.; Nakahara, H.; Saito, Y. Growth of non-concentric graphene ring on 6H-SiC (0001) surface. *Appl. Surf. Sci.* **2014**, *307*, 136−141.

(12) Ruammaitree, A.; Nakahara, H.; Saito, Y. Growth of protrusive graphene rings on Siterminated 6H−SiC (0001). *Surf. Interface Anal.* **2014**, *46*, 1156−1159.

(13) Ma, Y.; Lu, S.; Han, G.; Liu, Y.; Chen, Z. Chemical vapor deposition of two-dimensional molybdenum nitride/graphene van der Waals heterostructure with enhanced electrocatalytic hydrogen evolution performance. *Appl. Surf. Sci.* **2022**, *589*, No. 152934.

(14) Li, N.; Zhen, Z.; Xu, Z.; Zhang, R.; Mu, R.; He, L. The growth of large-sized graphene domains by Faraday cage-assisted plasma enhanced chemical vapor deposition. *Appl. Surf. Sci. Adv.* **2021**, *6*, No. 100154.

(15) Ruammaitree, A. Improvement in corrosion resistance of stainless steel foil by graphene coating using thermal chemical vapor deposition. *Surf. Rev. Lett.* **2018**, No. 1840003.

(16) Mangaiyarkarasi, R.; Santhiya, N.; Umadevi, S. Ionic liquid crystal − mediated preparation of reduced graphene oxide under microwave irradiation. *Colloids Surf., A* **2022**, *642*, No. 128673.

(17) Tienne, L. G. P.; Candido, L. S.; Cruz, B. S. M.; Gondim, F. F.; Ribeiro, M. P.; Simao, R. A.; Marques, M. F. V.; Monteiro, S. N. Reduced graphene oxide synthesized by a new modified Hummer's method for enhancing thermal and crystallinity properties of Poly (vinylidene fluoride). *J. Mater. Res. Technol.* **2022**, *18*, 4871−4893.

(18) Li, Y.; Gai, T.; Shao, L.; Tang, H.; Li, R.; Yang, S.; Wang, S.; Wu, Q.; Ren, Y. Synthesis of sandwich-like Mn3O4@reduced graphene oxide nano-composites via modified Hummers' method and its application as uranyl adsorbents. *Heliyon* **2019**, *5*, No. e01972.

(19) Wei, C.; Negishi, R.; Ogawa, Y.; Akabori, M.; Taniyasu, Y.; Kobayashi, Y. Turbostratic multilayer graphene synthesis on CVD graphene template toward improving electrical performance. *Jpn. J. Appl. Phys.* **2019**, *58*, SIIB04.

(20) Liu, K.; Lu, F.; Li, K.; Xu, Y.; Ma, C. Synthesis of turbostratic graphene by direct carbon ions implantation on $LiNbO_3$. *Appl. Surf. Sci.* **2019**, *493*, 1255−1259.

(21) Athanasiou, M.; Samartzis, N.; Sygellou, L.; Dracopoulos, V.; Ioannides, T.; Yannopoulos, S. N. High-quality laser-assisted biomass-based turbostratic graphene for high-performance supercapacitors. *Carbon* **2021**, *172*, 750−761.

(22) Wyss, K. M.; Wang, Z.; Alemany, L. B.; Kittrell, C.; Tour, J. M. Bulk Production of Any Ratio 12C:13C Turbostratic Flash Graphene and Its Unusual Spectroscopic Characteristics. *ACS Nano* **2021**, *15*, 10542−10552.

(23) Wyss, K. M.; Kleine, R. D. D.; Couvreur, R. L.; Kiziltas, A.; Mielewski, D. F.; Tour, J. M. Upcycling end-of-life vehicle waste plastic into flash graphene. *Commun. Eng.* **2022**, *1*, 1−12.

(24) Wyss, K. M.; Chen, W.; Beckham, J. L.; Savas, P. E.; Tour, J. M. Holey and Wrinkled Flash Graphene from Mixed Plastic Waste. *ACS Nano* **2022**, *16*, 7804−7815.

(25) Hu, X. H.; Zhang, R.; Wu, Z.; Xiong, S. Concentrated Solar Induced Graphene. *ACS Omega* **2022**, *7*, 27263−27271.

(26) Surinlert, P.; Kokmat, P.; Ruammaitree, A. Growth of turbostratic stacked graphene using waste ferric chloride solution as a feedstock. *RSC Adv.* **2022**, *12*, 25048−25053.

(27) Khezr, S. H.; Yazdani, A.; Khordad, R. Pure iron nanoparticles prepared by electric arc discharge method in ethylene glycol. *Eur. Phys. J. Appl. Phys.* **2012**, *59*, 30401.

(28) Ruammaitree, A.; Nakahara, H.; Akimoto, K.; Soda, K.; Saito, Y. Determination of non-uniform graphene thickness on SiC (0001) by X-ray diffraction. *Appl. Surf. Sci.* **2013**, *282*, 297−301.

(29) Brown, P.; Fox, A.; Maslen, E.; O'Keefe, M.; Willis, B.Atomic scattering factor. *International table for crystallography*, 3rd ed.; Prince, E., Ed.; The international union of crystallography: London, 2004, *C*, 555.

(30) Malard, L. M.; Pimenta, M. A.; Dresselhaus, G.; Dresselhaus, M. S. Raman spectroscopy in graphene. *Phys. Rep.* **2009**, *473*, 51−87.

(31) Allen, M. J.; Tung, V. C.; Kaner, R. B. Honeycomb Carbon: A Review of Graphene. *Chem. Rev.* **2010**, *110*, 132−145.

(32) Casiraghi, C. Doping dependence of the Raman peaks intensity of graphene close to the Dirac point. *Phys. Rev. B* **2009**, *80*, No. 233407.

(33) Matthews, M. J.; Pimenta, M. A.; Dresselhaus, G.; Dresselhaus, M. S.; Endo, M. Origin of dispersive effects of the Raman D band in carbon materials. *Phys. Rev. B* **1999**, *59*, R6585−R6588.

(34) Liu, Y. L.; Yu, C. C.; Fang, C. Y.; Chen, H. L.; Chen, C. W.; Kuo, C. C.; Chang, C. K.; Chen, L. C.; Chen, K. H. Using Optical

Anisotropy as a Quality Factor to Rapidly Characterize Structural Qualities of Large-Area Graphene Films. *Chen. Anal. Chem.* **2013**, *85*, 1605−1614.
(35) Senneca, O. Oxidation of carbon: what we know and what we still need to know. *Energy Procedia* **2017**, *120*, 62−74.
(36) Zhou, L.Chapter 3 − Fundamentals of Combustion Theory. *Theory and Modeling of Dispersed Multiphase Turbulent Reacting Flows*; Butterworth-Heinemann2018, 15−70, DOI: 10.1016/B978-0-12-813465-8.00003-X.
(37) Ruammaitree, A.; Phokharatkul, D.; Wisitsoraat, A. Surface Hardening of Stainless Steel by Coating Graphene Using Thermal Chemical Vapor Deposition. *Solid State Phenom.* **2018**, *283*, 173−178.
(38) Pimenta, M. A.; Dresselhaus, G.; Dresselhaus, M. S.; Cancado, L. G.; Jorioa, A.; Saito, R. Studying disorder in graphite-based systems by Raman spectroscopy. *Phys. Chem. Chem. Phys.* **2007**, *9*, 1276−1290.
(39) Cancado, L. G.; Takai, K.; Enoki, T.; Endo, M.; Kim, Y. A.; Mizusaki, H.; Speziali, N. L.; Jorio, A.; Pimenta, M. A. Measuring the degree of stacking order in graphite by Raman spectroscopy. *Carbon* **2008**, *46*, 272−275.
(40) Cong, C.; Yu, T.; Saito, R.; Dresselhaus, G. F.; Dresselhaus, M. S. Second-Order Overtone and Combination Raman Modes of Graphene Layers in the Range of 1690-2150 cm^{-1}. *ACS Nano* **2011**, *5*, 1600−1605.
(41) Rao, R.; Podila, R.; Tsuchikawa, R.; Katoch, J.; Tishler, D.; Rao, A. M.; Ishigami, M. Effects of Layer Stacking on the Combination Raman Modes in Graphene. *ACS Nano* **2011**, *5*, 1594−1599.
(42) Gupta, N.; Walia, S.; Mogera, U.; Kulkarni, G. U. Twist-Dependent Raman and Electron Diffraction Correlations in Twisted Multilayer Graphene. *J. Phys. Chem. Lett.* **2020**, *11*, 2797−2803.
(43) Rabchinskii, M. K.; Saveliev, S. D.; Stolyarova, D. Y.; Brzhezinskaya, M.; Kirilenko, D. A.; Baidakova, M. V.; Ryzhkov, S. A.; Shnitov, V. V.; Sysoev, V. V.; Brunkov, P. N. Modulating nitrogen species via N-doping and post annealing of graphene derivatives: XPS and XAS examination. *Carbon* **2021**, *182*, 593−604.

https://doi.org/10.1021/acsomega.2c06834
ACS Omega 2023, 8, 4010−4018